Electronic Supplementary Information

Ultrahigh Pressure Synthesis of Highly Efficient FeN_x/C Electrocatalysts for Oxygen Reduction Reaction

Xin Guo,[a,b] Xiaopeng Jia,[c] Ping Song,[a] Jing Liu,[a,d] Erling Li,[a,d]Mingbo Ruan[a] and Weilin Xu[a,*]

[a]State Key Laboratory of Electroanalytical Chemistry & Jilin Province Key Laboratory of Low Carbon Chemical Power, Changchun Institute of Applied Chemistry, Chinese Academy of Sciences.

[b]Department of Materials Science and Engineering, Changchun University of Science and Technology, 7989 Weixing Road, Changchun, 130022, P. R. China

[c]State Key Laboratory of Superhard Materials, Jilin University, 2699 Qianjin Street, Changchun, 130012, P. R. China

[d]University of Chinese Academy of Sciences, Beijing, 100049, P. R. China

*Corresponding author. E-mail: weilinxu@ciac.ac.cn

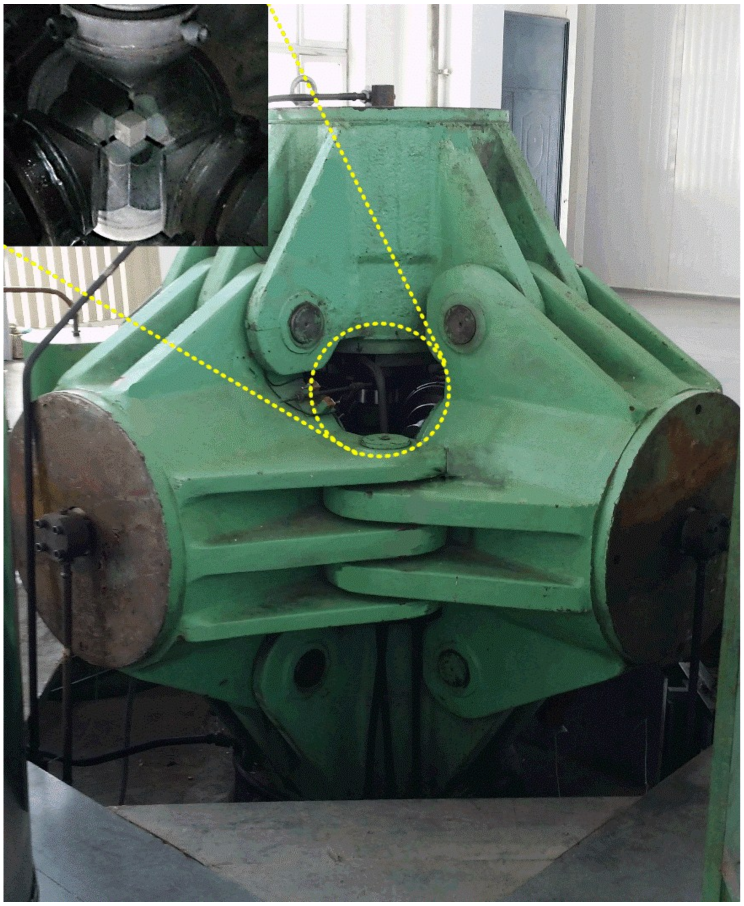

Figure S1. The image of a cubic anvil high-pressure apparatus (SPD 6×1200), the inset is pressure cavity with a sample chamber. Ultrahigh pressure for cubic sample chamber can be realized by six cemented carbides squeezing six surfaces of cubic chamber with a sample simultaneously. The synthesis temperature can be realized simultaneously by conducting current to go through a graphite box in chamber, as a heating unit, with a sample.

As for the reference electrode adopted here, in our three-electrode system, we adopted a special salt-bridge as shown in the following Fig. S2. In such system, a short Pt wire was sealed at the end of a glass capillary but with the two end of the wire exposed to the air (Fig. S2a), then the solution of KCl electrolyte in the capillary was separated tightly from the outer alkaline solution, that means with such special salt bridge, the outer solution will never contaminate the reference electrode.

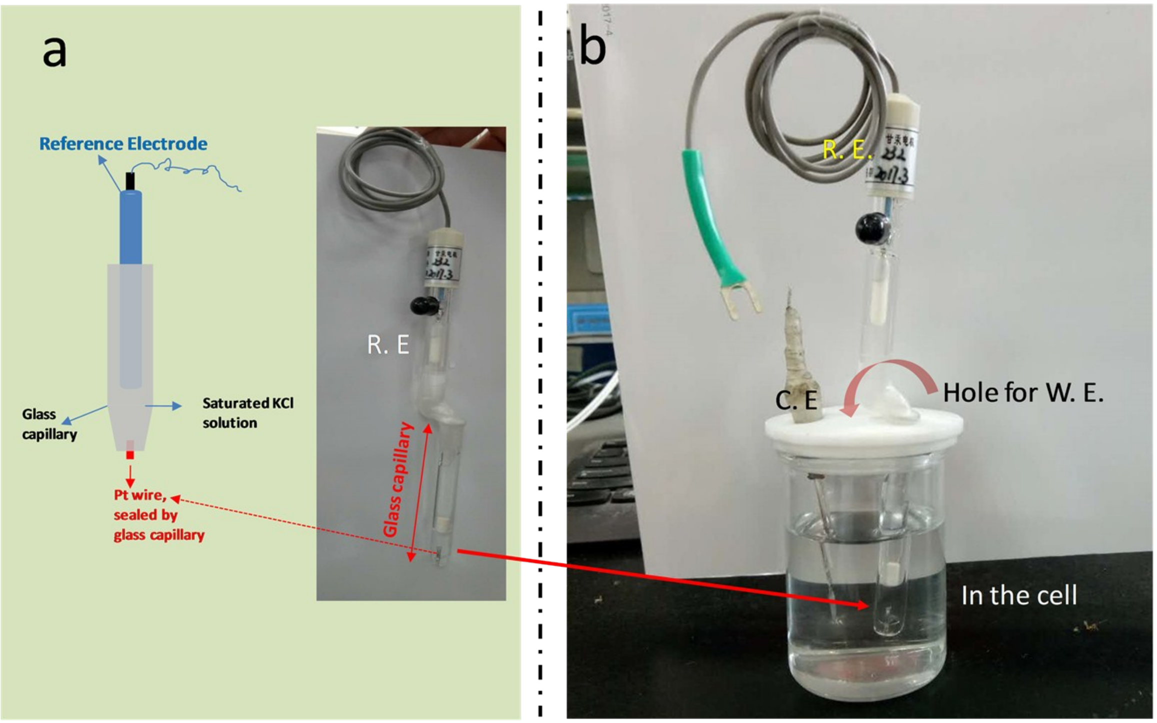

Figure S2. (a) Scheme to show the reference electrode system with a special salt bridge, right: real image of R. E. connected with the special salt bridge. (b) Real image of the reference electrode in the cell for three-electrode test.

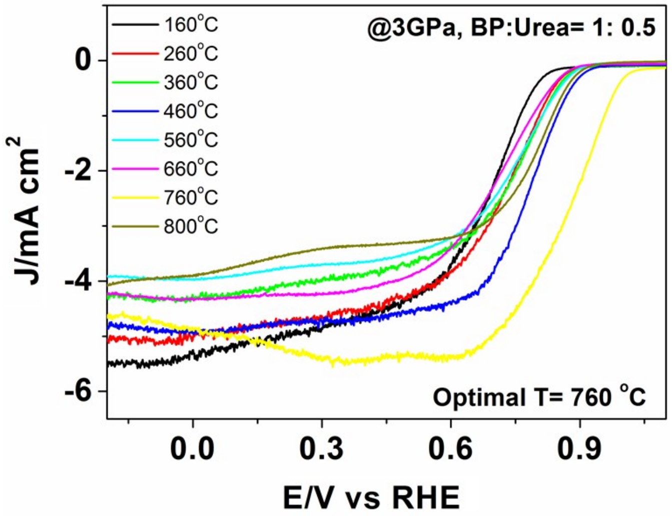

Figure S3. The temperature optimization based on fixed pressure of 3GPa and the mass ratio of BP: urea= 1: 0.5.

In order to prevent NH_3 gas leakage (the decomposition of urea under temperature) and experimental safety for the sealed sample chamber, a safe pressure, which is 3GPa, has been randomly chosen to conduct initial optimization of synthetic condition. It can clearly observe that Figure S3 shows clearly that the optimal temperature is 760°C.

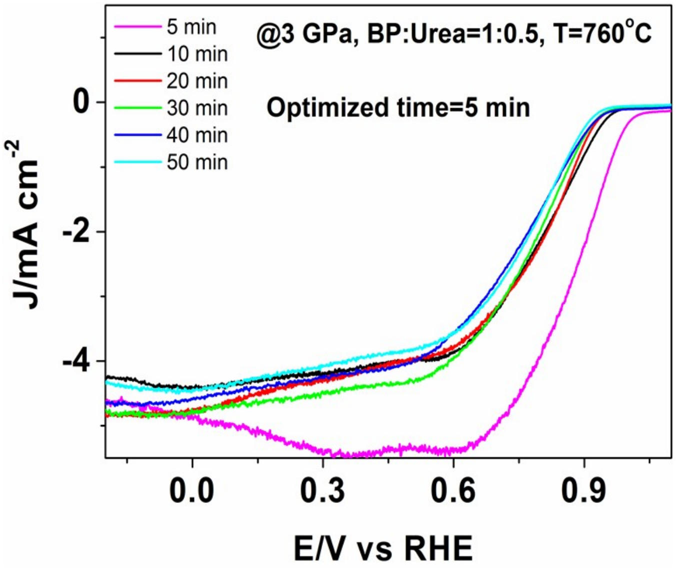

Figure S4. The time optimization based on fixed pressure of 3GPa, optimized temperature of 760°C and the mass ratio of BP: urea= 1: 0.5.

Figure S4 shows clearly that the optimized time is 5 minutes.

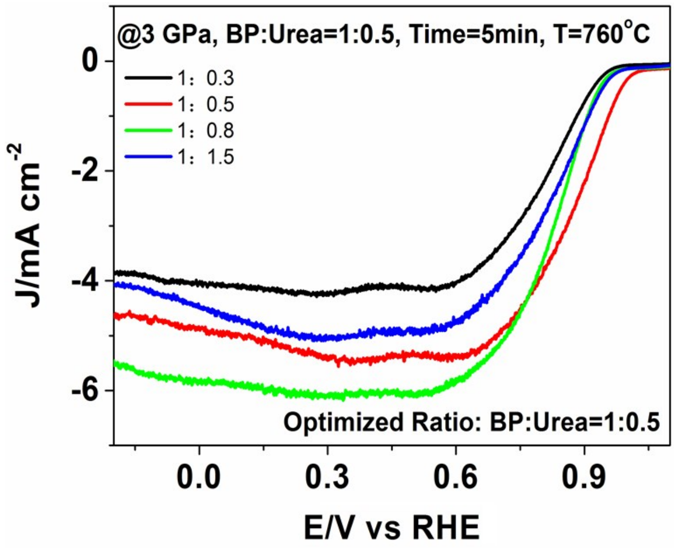

Figure S5. The optimization of the mass ratio between carbon BP and the urea based on fixed pressure of 3GPa, optimized temperature of 760°C and pyrolysis time of 5min. It shows clearly that the optimal mass ratio of BP: urea= 1: 0.5.

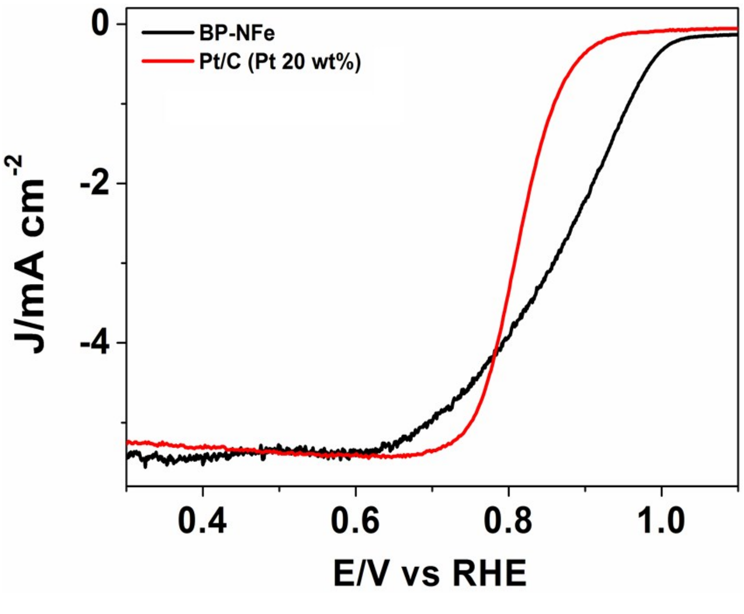

Figure S6. The comparison of ORR activity between BP-NFe and commercial Pt/C with Pt 20 wt% in oxygen-saturated 0.1 M KOH.

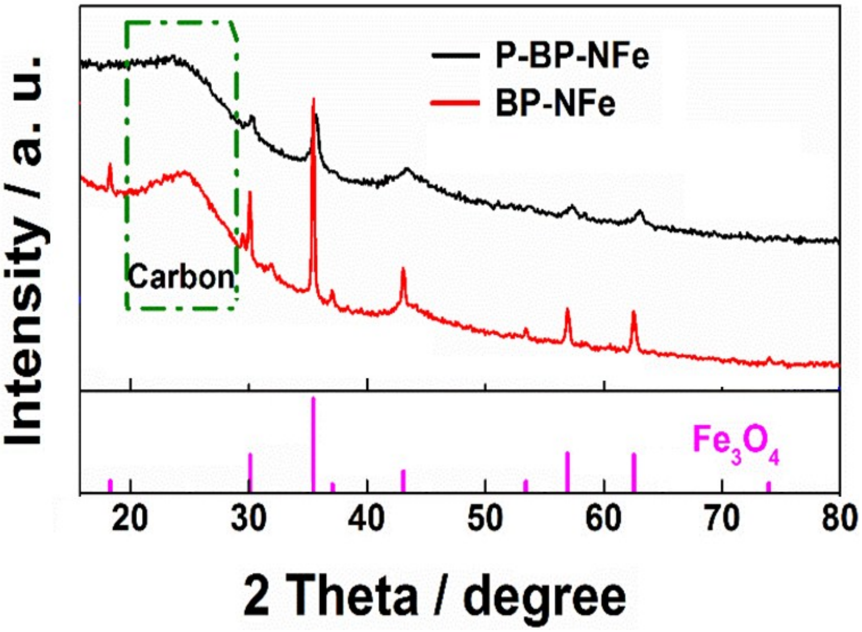

Figure S7. The XRD analysis of BP-NFe and P-BP-NFe. It shows clearly that the Fe_3O_4 is the main form of iron on these catalysts.

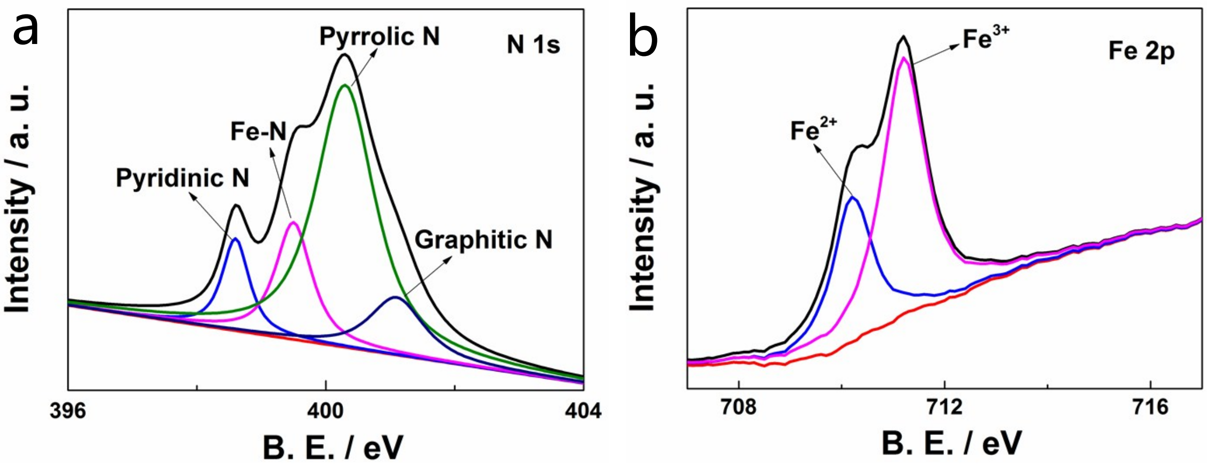

Figure S8. High-resolution XPS spectra of N 1s (a) and Fe 2p (b) of the P-BP-NFe catalyst.

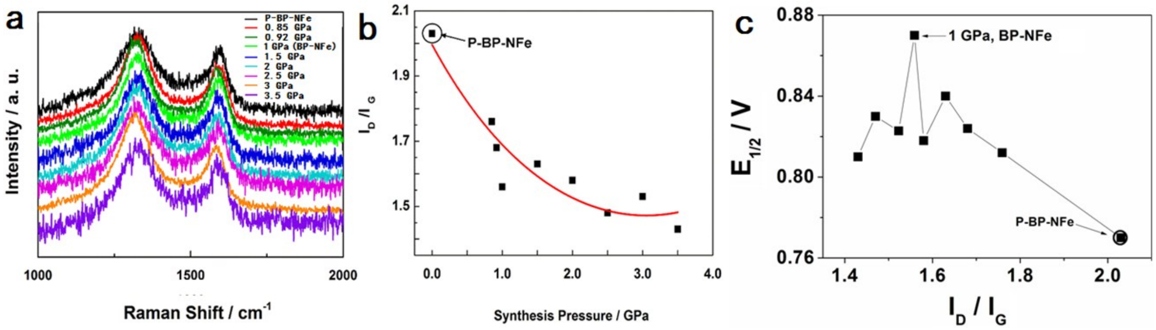

Figure S9. (a)Raman spectra of P-BP-NFe and BP-NFe catalysts prepared under UHP from 0.85 to 3.5GPa. (b) Pressure-dependence of I_D/I_G. (c) I_D/I_G -dependence of $E_{1/2}$.

Fig. S9 shows the Raman spectra and obtained the relative intensities between D band and G band (ID/IG) for all the catalysts prepared under different pressures. As shown in the Fig. S9, interestingly, the value of ID/IG decreases gradually with the increase of pressure(Fig. S9b), consistent with the results shown in Fig. 4c. Such result indicates that the UHP can substantially enhance the graphitization degree of carbon in the catalysts. From the relationship between the half-wave potential ($E_{1/2}$) and the corresponding ID/IG (Fig. S9c), one can see, at low pressure, the slight enhancement of graphitization can improve the ORR activity due to the improvement of the electronic conductivity and corrosion resistance of catalysts. However, with the further enhancement of graphitization induced by high pressure, the ORR performance decreased inversely due to the decrease of BET surface area and pore size induced by UHP as shown in Fig. 3c,d. Such fact indicates that the BET surface area and pore size contribute more to ORR activity of the catalyst than the graphitization does.

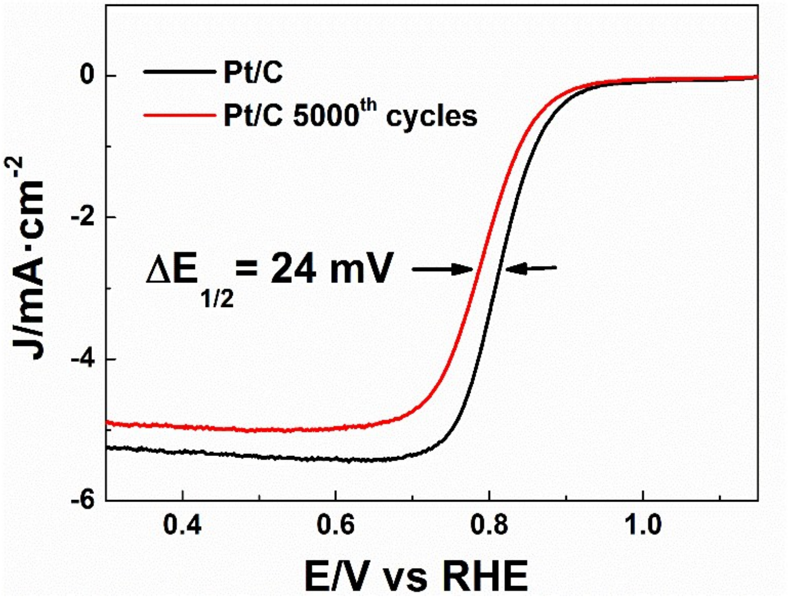

Figure S10. LSV curves of commercial Pt/C (Pt 20wt%) with a scan rate of 5mV/s before and after 5000 potential cycles in O_2 saturated 0.1M KOH. The Pt loading is 24μg/cm^2.

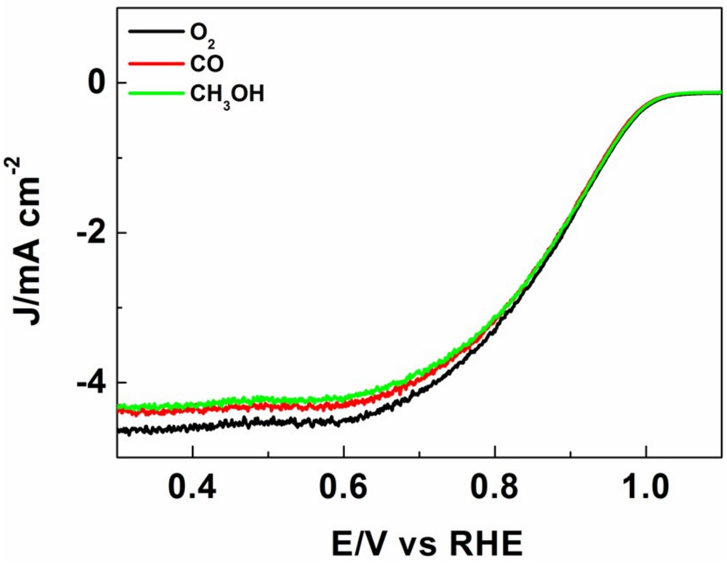

Figure S11. The LSV curves for BP-NFe before and after CO and methanol poisoning in O_2-saturated 0.1 M KOH.

Table S1. A benchmark of our optimal BP-NFe with performance obtained from some other independent literatures. All in alkaline condition with 0.1 M KOH.

Source/References	**Loading (mg/cm^2)**	**Activity vs. RHE**
This work (FeN_x/C catalyst)	0.39	E_{onset}=1.06 V $E_{1/2}$=0.87 V
Nat. Commun. 2013, 4, 2076 (N, Fe co-doped carbon nanotubes)	0.32	E_{onset}≈1.0V $E_{1/2}$≈0.90 V
Nat. Commun. 2013, 4, 1922 (N, Fe co-doped carbon black)	1.0	$E_{1/2}$≈0.89 V
Nat. Commun. 2015, 6, 8618 ((Fe,Mn)-N-C-3HT-2AL)	0.8	E_{onset}=0.98 V $E_{1/2}$=0.90 V
Nat. Nanotechnol. 2012, 7, 394 (NT-G)	0.49	E_{onset}≈1.05 V
J. Am. Chem. Soc. 2015, 137, 5555 (Fe-N/C-800)	0.08	E_{onset}=0.98 V
J. Am. Chem. Soc. 2015, 137, 1436 (Fe, N co-doped carbon)	1.2	$E_{1/2}$=0.86 V
J. Am. Chem. Soc. 2014, 136, 11027 (Fe-N/C-800)	0.1	E_{onset}=0.92 V $E_{1/2}$=0.81 V
J. Am. Chem. Soc. 2014, 136, 14486	0.8	E_{onset}= 0.93 V

(S/N_Fe27)		
J. Am. Chem. Soc., 2016, 138, 15046 (CNT/PC)	0.8	$E_{1/2}$=0.88 V
Adv. Mater. 2017,1606534 (N, Feco-doped carbon)	0.2	E_{onset}=0.95 V $E_{1/2}$=0.86 V
Adv. Mater. 2016, 28, 7948 (Fe, N co-doped carbon)	0.26	E_{onset}=1.02 V $E_{1/2}$=0.86 V
Adv.Mater.2015,27,2521 (Fe, N co-doped carbon)	0.4	E_{onset}=1.03 V $E_{1/2}$=0.86 V
Adv. Mater. 2013, 25, 6879 (Fe, N co-doped carbon black)	0.39	E_{onset}≈1.02 V $E_{1/2}$≈0.89 V
Angew. Chem. In. Ed. 2017, 56, 1 (Fe, N co-doped carbon)	0.41	E_{onset}=0.98 V $E_{1/2}$=0.90 V
Angew. Chem. In. Ed. 2014,53, 3675 (Fe_3/C-800 with trace N)	0.6	E_{onset}=1.05 V $E_{1/2}$= 0.83 V
Angew. Chem. Int. Ed 2014, 53, 6659 ((DFTPP)Fe-Im-CNTs)	1.0	$E_{1/2}$=0.922 V
Nano Lett. 2017, 17, 2003 (Fe-N-SCCFs)	0.24	E_{onset}=1.03 V $E_{1/2}$=0.883 V
Sci. Rep. 2013, 3, 2715 (FeCo-OMPC)	0.3	No mention
ACS Nano 2016, 10, 5922 (Fe, N co-doped carbon)	0.10	E_{onset}≈0.94 V $E_{1/2}$≈0.83 V
J. Mater. Chem. A 2017, 5, 11340 (Fe-N-CNBs-600)	0.43	E_{onset}=1.03 V $E_{1/2}$=0.87 V
J. Mater. Chem. A 2017,DOI:10.1039/C7TA01896G (FeNCS-1000)	unknown	$E_{1/2}$=0.88 V
J. Mater. Chem. A 2017, 5,1930-1934 (Fe-N-CIG)	0.23	$E_{1/2}$=0.84 V

Table S2. The relative amount of different chemical states of doped N and Fe in catalysts.

	Pyridinic N	Pyrrolic N	Graphitic N	Fe-N	Fe^{2+}	Fe^{3+}	Fe^{2+} in Fe-N
BP-NFe	33.04%	26.64%	8.82%	31.50%	37.91%	62.09%	6.90%
P-BP-NFe	20.75 %	47.18 %	8.49 %	23.58 %	34.25 %	65.75 %	1.30%